Journal of Alloys and Compounds 505 (2010) 91–95

Contents lists available at ScienceDirect

Journal of Alloys and Compounds

journal homepage: www.elsevier.com/locate/jallcom

Nucleation rate and nanocrystallization of Co_{60}–$(Fe, Mn)_{18}$–Nb_6–B_{16} amorphous alloys in the frame of instantaneous growth approximation

J.S. Blázquez, M. Millán, C.F. Conde, A. Conde*

Departamento de Física de la Materia Condensada, ICMSE-CSIC, Universidad de Sevilla, P.O. Box 1065, 41080, Sevilla, Spain

ARTICLE INFO

Article history:
Received 17 May 2010
Received in revised form 7 June 2010
Accepted 9 June 2010
Available online 18 June 2010

Keywords:
Amorphous and nanocrystalline materials
Nanocrystallization kinetics

ABSTRACT

Instantaneous growth approximation is based on the fact that the time required by a new nucleus to reach its saturation size is negligible in comparison with the time required for the whole crystallization process. This approximation has been applied to analyze the kinetics of the nanocrystallization process of $Co_{60}Fe_{18-x}Mn_xNb_6B_{16}$ ($x = 0$ and 4) alloys. Direct application of JMAK theory leads to divergences at very high transformed fractions. Although this divergence could be due to some artifacts, it can also be solved after a reinterpretation of the geometrical impingement effect on nanocrystalline systems. A modified Arrhenius relationship can be used for a general description of the double dependency of nucleation rate on the transformed fraction (only through the local activation energy) and the temperature.

© 2010 Elsevier B.V. All rights reserved.

1. Introduction

Fe based nanocrystalline microstructures obtained after controlled partial crystallization of suitable alloy compositions have attracted high interest from the scientific community especially since the discovery of FINEMET alloys by Yoshizawa et al. two decades ago [1]. Afterwards, other nanocrystalline alloy families appeared: the so-called NANOPERM [2] and HITPERM [3] alloys. The general description of the composition of these alloys is Fe(Co)–ET–M–(Cu), where Co is especially present in HITPERM alloys in order to enhance the high temperature performances [3]; ET is an early transition metal, such as Zr, Nb, Hf, etc., which, due to its low solubility in α-Fe and its slow diffusivity in the residual amorphous matrix, constrains the growth of the α-Fe crystallites by piling up at their boundaries; and M is a metalloid, mainly B and/or Si, which role is to reduce the cooling rate needed to obtain the amorphous alloy. Unlike B, Si is soluble in the α-Fe phase and, therefore, its addition reduces the Curie temperature and the saturation magnetization of the crystalline phase with respect to Si free alloys. These nanocrystalline microstructures consist of small α-Fe type crystallites (5–20 nm in size) with a high Curie temperature embedded in a residual amorphous matrix, also ferromagnetic but with a lower Curie temperature and enriched in those elements expelled out from the crystals (ET and B, for example). The two-phase character of the microstructure is the responsible for the outstanding soft magnetic properties exhibited by these alloys [4]. Nevertheless, nanocrystalline microstructures can be also observed in other alloys as those based on Al [5] or Zr [6] with excellent mechanical behaviour.

In general, the nanocrystalline microstructure is developed during a primary crystallization process from a precursor amorphous alloy. After further thermal treatments, this new metastable microstructure will change to a fully crystalline system. The extraordinarily strong impingement due to the piling up of the early transition metal at the edges of the crystallites [7] leads to a huge number of nuclei, several orders of magnitude higher than that found in conventional microstructures (with a grain size of the order of microns). In fact, for a nanocrystalline sample with only 50% of crystalline volume fraction with a nanocrystal size of 5 nm, the density of nuclei is $\sim 10^{25}$ m^{-3}. However for a 100% crystalline sample with micrometric crystals, the density of nuclei is $\sim 10^{18}$ m^{-3}. On the other hand, the size evolution of the nanocrystals is very limited: after a new nucleus is formed, it grows fast to an almost saturation value and no appreciable growth is observed unless high temperature transformation occurs (second stage of crystallization). Under these two premises, instantaneous growth approximation has been proposed to make a rough analysis of the nanocrystallization kinetics [8]. This approximation is based on the fact that the time required by a new nucleus to grow up to its saturation size is negligible with respect to the time involved in the whole nanocrystallization process. Therefore, kinetics related to growth processes is hidden by the most relevant nucleation phenomenon.

2. Kinetic theory

Once the growth process is simplified in such a way that crystals appear suddenly with their saturation size, kinetic results can be analyzed in the frame of Johnson–Mehl–Avrami–Kolmogorov

* Corresponding author. Tel.: +34 95 455 28 85; fax: +34 95 461 20 97.
E-mail address: conde@us.es (A. Conde).

0925-8388/$ – see front matter © 2010 Elsevier B.V. All rights reserved.
doi:10.1016/j.jallcom.2010.06.045

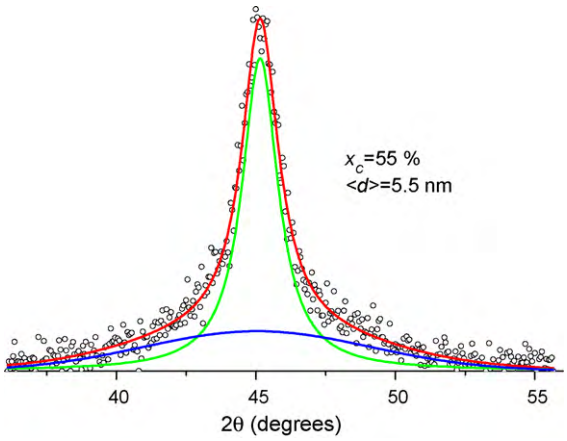

Fig. 1. XRD pattern of the alloy with 4 at.% of Mn at the end of the nanocrystallization process showing the deconvolution used. Blue line corresponds to the amorphous halo (fitted as a Gaussian); green line corresponds to the (1 1 0) diffraction maximum of the bcc Co, Fe phase (fitted as a Lorentzian) and red line is the sum of both contributions. (For interpretation of the references to color in this figure legend, the reader is referred to the web version of the article.)

(JMAK) theory [9] reducing the Avrami exponent, n, to $n = n_I$, where n_I refers to nucleation process. The original JMAK theory considers polymorphic transformations and the parent and product phases have the same composition. However, in nanocrystallization processes this fact is not fulfilled and a partial transformation occurs. In order to overcome this fact, the transformed fraction is normalized to be 1 at the end of the nanocrystallization process. Therefore, it is worth distinguishing between two different magnitudes characterizing the transformation: crystalline volume fraction, x_C, which is an actual crystalline fraction, with a maximum value below 1; and transformed fraction, X, which is 1 at the end of the nanocrystallization process. The relationship between both magnitudes is:

$$X = \frac{x_C}{x_C^{MAX}} \tag{1}$$

The parameter to be used in JMAK expressions is the normalized X. On the other hand, JMAK theory considers the so-called geometrical impingement [10], which takes into account that a crystal cannot grow further on an already transformed region. In order to evaluate this factor, a new magnitude is defined as the extended volume fraction X^*, which does not consider the geometrical impingement but is easily calculated by adding up the number of nuclei formed and growing at a characteristic rate. Under the instantaneous growth approximation, the value of X^* is reduced to:

$$X^* = \int_0^t \frac{v_c}{x_C^{MAX}} I(X, T)\, dt \tag{2}$$

where $I(X, T)$ is the nucleation rate, $v_C = \pi/6\langle d\rangle^3$ is the average volume of a formed nanocrystal and $\langle d\rangle$ its average diameter. This equation can be expressed in a differential form as:

$$\frac{dX^*}{dt} = \frac{\pi}{6x_C^{MAX}} \langle d\rangle^3 I(X, T) \tag{3}$$

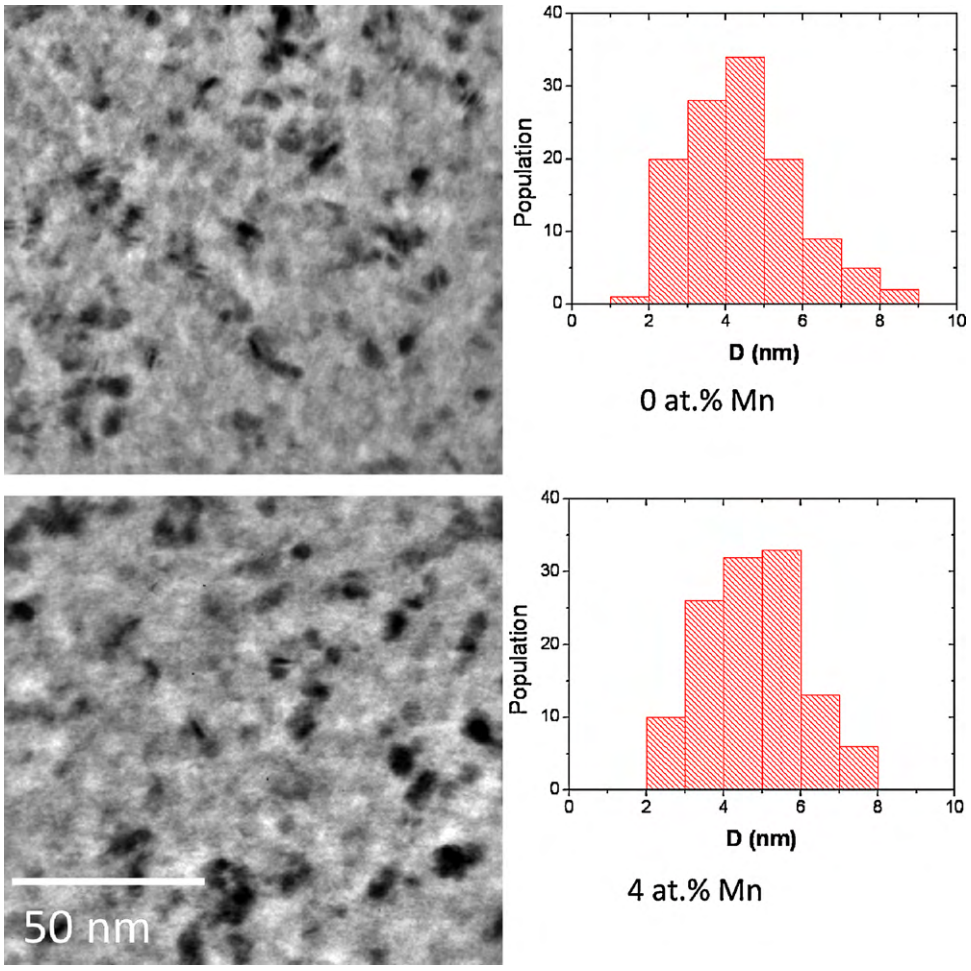

Fig. 2. Bright field image and crystal size distribution of 0 and 4 at.% Mn alloys heated up to the end of the nanocrystallization process.

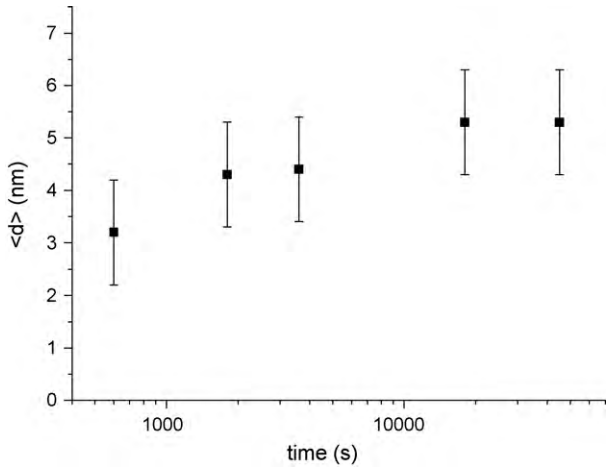

Fig. 3. Crystal size evolution during isothermal annealing at 35 K below the onset for the Mn free alloy.

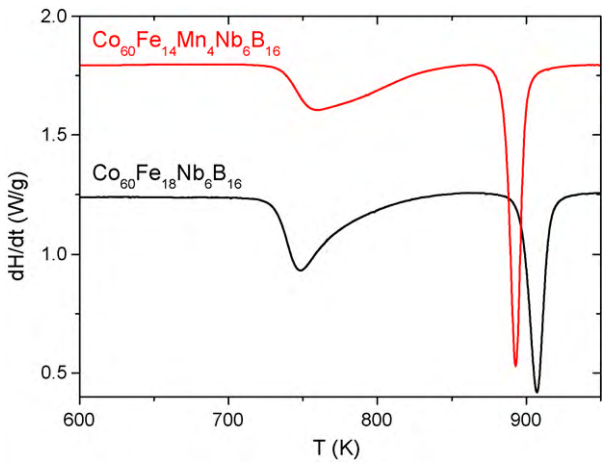

Fig. 4. DSC scans at 10 K/min of amorphous samples of the two studied alloys.

On the other hand, JMAK theory links the extended transformed fraction with the transformed fraction through:

$$\frac{dX}{dX^*} = (1 - X) \tag{4}$$

This indicates that, although the extended transformed fraction can increase continuously, the saturation value of the transformed fraction is 1.

Combining Eqs. (3) and (4) it can be derived a direct relationship between the rate of transformation, dX/dt, and the nucleation rate, I:

$$I(X,T) = \frac{6x_C^{MAX}}{\pi \langle d \rangle^3} \frac{1}{1-X} \frac{dX}{dt} \tag{5}$$

Eq. (5) has been applied to the nanocrystallization process of $Co_{60}Fe_{18-x}Mn_xNb_6B_{16}$ ($x = 0$ and 4) alloys, obtained by rapid quenching. Small addition of Mn in these alloys has a strong effect in the composition of the nanocrystals with respect to other analogous Fe and Co containing nanocrystalline alloys. In general, during nanocrystallization, Co is homogeneously distributed throughout the amorphous matrix and the α-Fe, Co(Si) nanocrystals without any preferential partitioning [11–13]. This fact leads to an exhaustion of Fe in the amorphous matrix for the alloys with high Co content that stops the nanocrystallization process [14]. However, after small substitution of Mn for Fe, the nanocrystals become enriched in Co too, leading to larger crystalline volume fractions at the end of the nanocrystallization than in the case of Mn free alloy [15].

3. Experimental

In order to apply Eq. (5), x_C was measured from X-ray diffraction (XRD) patterns of samples at the end of the nanocrystallization process using Cu Kα wavelength. Deconvolution of the (1 1 0) peak of the α-Fe, Co(Mn) phase and the amorphous halo leads to $x_C \sim 55$ and ~43% for the alloys with Mn and without Mn, respectively, after correcting the different scattering power of the crystalline and amorphous phases.

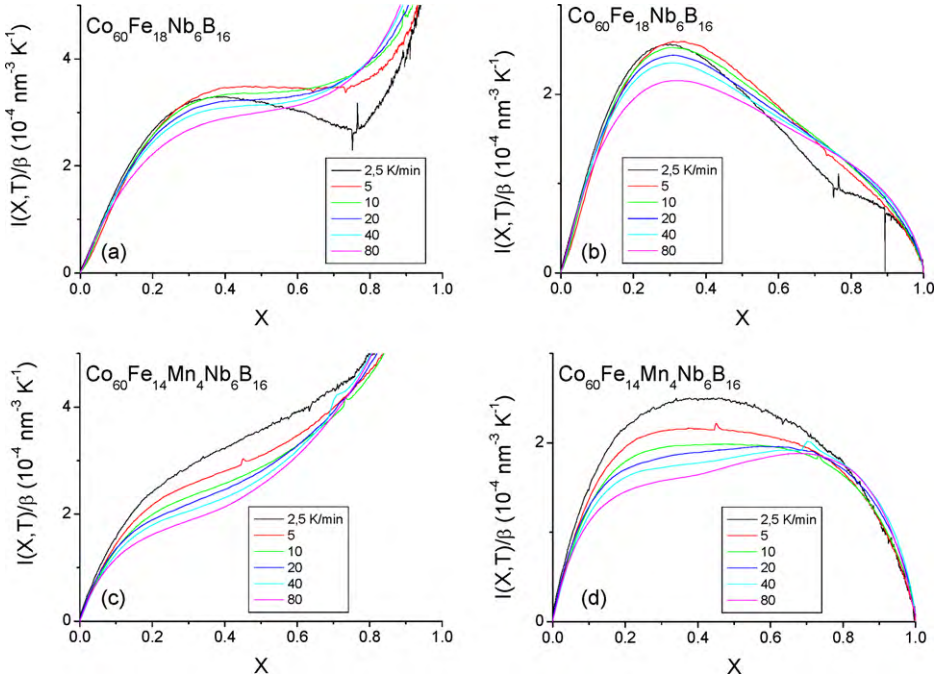

Fig. 5. Nucleation rates obtained from DSC curves at different heating rates for the 0, (a) and (b), and 4 at.% Mn alloy, (c) and (d). Without correcting the transformed fraction (using Eq. (5)), (a) and (c), and correcting the transformed fraction to the crystalline volume fraction (using Eq. (6)), (b) and (d). Results are shown after normalizing using the heating rate.

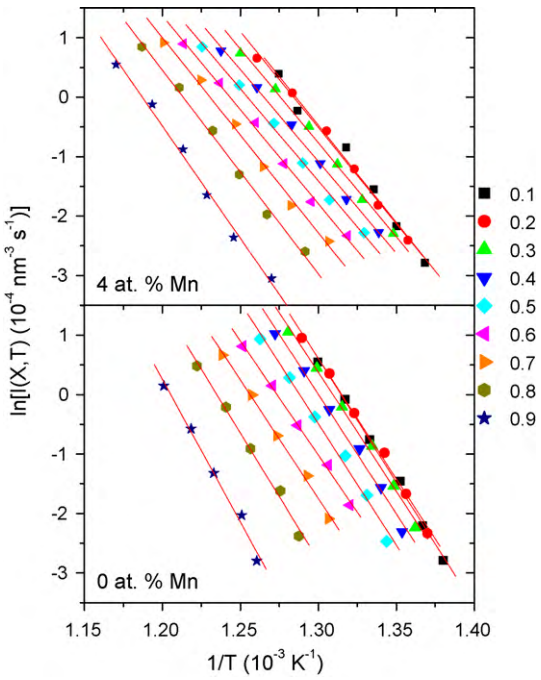

Fig. 6. Logarithm of the nucleation rate versus the inverse of the temperature for different values of the transformed fraction.

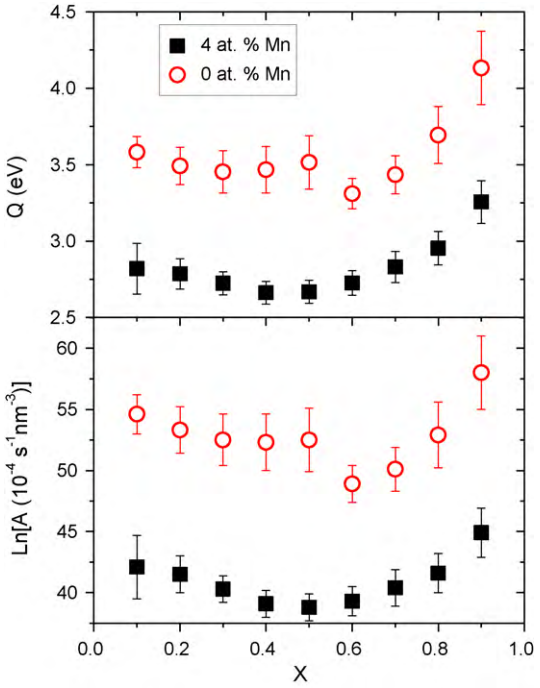

Fig. 7. Local activation energy (above) and logarithm of the prefactor of the Arrhenius relationship (below) versus the transformed fraction.

An average value of the crystal size could be also obtained from Scherrer formula. As an example, Fig. 1 shows the deconvoluted XRD maximum for the Mn containing alloy.

A more detailed analysis on the nanocrystal size was performed from transmission electron microscopy (TEM) using a Philips CM200 at 200 kV. Fig. 2 shows similar TEM bright field images as well as grain size distribution histograms for the two studied alloys. Fig. 3 shows the grain size evolution for the Mn free alloy as a function of isothermal annealing time at 35 K below the onset of crystallization. It is worth mentioning the logarithmic scale of the time axis. Although a limited evolution is found, it is in the range of the error bar and only at very low annealing times. Moreover, there is an artifact in TEM measurements which could yield a fictitious increase of the average size of the nanocrystals as the crystalline fraction increases: in fact, as the number of crystallites per image area increases, overlapping between crystals becomes more probable and two (or more) crystallites could be interpreted as a single one with a larger size.

In the present study, non-isothermal annealing in a Perkin-Elmer DSC7 differential scanning calorimeter (DSC) at different heating rates were used to obtain the transformation rate after normalizing the heat flow signal using the total enthalpy under the exothermic peak ascribed to the nanocrystallization process. As an example, Fig. 4 shows the DSC plots at 10 K/min for the two studied compositions. Considering the transformed fraction to be proportional to the enthalpy has been criticized [16], especially at the end of the nanocrystallization. However, other techniques to obtain the crystalline fraction as TEM, resistivity, etc. do not lack of similar criticisms or even other specific ones (for example the non equal thickness in different TEM images). The use of DSC data supplies a continuous kinetic plot very simple to handle.

4. Results and discussions

The nucleation rates as a function of the transformed fraction obtained from Eq. (5) are plotted in Fig. 5(a) and (c) for Mn free and Mn containing alloys, respectively (in order to compare data obtained at different heating rates, nucleation rate has been divided by the corresponding heating rate). Results are similar for both alloys below $X = 0.2$, with an almost linear increase of the nucleation rate, which reaches higher values for the Mn free alloy than in the alloy with Mn, indicating a more difficult start of the nucleation process in the alloy with less Fe content. After this initial increase, whereas for Mn free alloy the nucleation rate is roughly constant from $0.2 < X < 0.7$, for the Mn containing alloy, nucleation rate continuously increases independently of the heating rate. At higher transformed fraction, $X > 0.8$, nucleation rate diverges, which has no physical meaning but can be due to several artifacts: errors in the baseline determination or fails on the proportionality between the DSC signal and the actual transformation rate, for example. However, there is another feature which could affect the nucleation rate plots calculated and this is linked to the geometrical impingement which led to the definition of the extended transformed fraction in JMAK theory. Using Eq. (5) implicitly assumes that at $X = 1$, geometrical impingement will occur for any further transformation. However, nanocrystallization process does not stop due to geometrical impingement as, at the end of the process, individual crystals can be observed to be well separated from others by a thin layer of amorphous matrix (see Fig. 2). If actual geometrical impingement is assumed, Eq. (5) will change to:

$$I(X,T) = \frac{6x_C^{MAX}}{\pi\langle d\rangle^3}\frac{1}{1-x_C}\frac{dX}{dt} = \frac{6x_C^{MAX}}{\pi\langle d\rangle^3}\frac{1}{1-(x_C^{MAX}\cdot X)}\frac{dX}{dt} \quad (6)$$

where the transformed fraction X is substituted by the actual crystalline fraction $x_C = x_C^{MAX}\cdot X$. If this is done, nucleation rates of Fig. 5(a) and (c) change to those of Fig. 5(b) and (d) for the Mn free and the Mn containing alloys, respectively. The corrected nucleation rate solves the divergences at high transformed fractions, being now down to zero as X goes to 1. The values of $I(X, T)$ at low transformed fractions do not change significantly and, for both alloys, a linear increase is observed. The transformed fraction at which the maximum nucleation rate is obtained remains independent of the heating rate (at $X = 0.31$) for Mn free alloy, in agreement with an isokinetic behaviour. However, for the Mn containing alloy a continuous increase from $X = 0.39$ to 0.68 is found as β increases from 2.5 to 80 K/min.

An important effect that can be invoked to explain the non-constant nucleation is the compositional changes that must occur during the transformation. Initially, expelling out of Nb from the forming nuclei to the edges might yield diffusion of Fe and Co in the amorphous phase. This could enhance compositional fluctuations which would be responsible of an initial increase of the nucleation rate. However, the amorphous matrix becomes poorer in the ele-

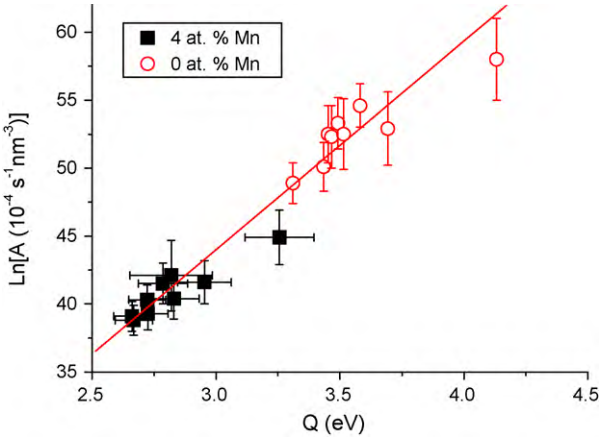

Fig. 8. Logarithm of the prefactor of the Arrhenius relationship versus the corresponding activation energy.

ments needed to form new nuclei as the crystallization progresses and this fact could explain the decay in the nucleation rate observed at high values of the transformed fraction.

A simple Arrhenius relationship could be proposed to describe the nucleation rate as a thermally activated process.

$$I(X,T) = A(X)\exp\left[-\frac{Q(X)}{RT}\right] \tag{7}$$

where Q is the local activation energy and A is a prefactor and both magnitudes depend on the transformed fraction. R is the gas constant and T, the temperature. Fig. 6 shows the linear fittings for $\ln[I(X,T)]$ versus $1/T$ for several values of X for both alloys. From these linear fittings, $Q(X)$ and $\ln[A(X)]$ were obtained and are represented in Fig. 7. Both magnitudes are correlated as it is shown in Fig. 8. In this figure, $\ln[A(X)]$ is plotted versus $Q(X)$. All the data, including both alloys, fulfill a linear relationship:

$$\ln[A(X)] = \ln[I_0] + \frac{Q(X)}{R\theta} \tag{8}$$

where I_0 has the units of the nucleation rate and the slope is $1/R\theta$, where θ has temperature units. This relationship yields a modification of expression (7) to:

$$I(X,T) = I_0\exp\left[\frac{Q(X)}{R\theta}\left(\frac{T-\theta}{T}\right)\right] \tag{9}$$

where $\theta = 760 \pm 50$ K should be a common value for both alloys. It is worth mentioning that this behavior was previously reported for the devitrification of some amorphous alloys [17,18] and similar values of θ appear from isothermal kinetic analysis of $Fe_{60}Co_{18}Nb_6B_{16}$ alloy [19].

5. Conclusions

Instantaneous growth approximation has been applied to analyze the kinetics of the nanocrystallization process of two alloys: $Co_{60}Fe_{18-x}Mn_xNb_6B_{16}$ ($x = 0$ and 4).

Application of JMAK theory without correction leads to divergences at very high transformed fractions. Although this divergence could be due to some artifacts, it can also be solved after a reinterpretation of the geometrical impingement effect on nanocrystalline systems.

A modified Arrhenius relationship can be used for a general description of the double dependency of nucleation rate on the transformed fraction (only through the local activation energy) and the temperature.

Further studies on systems which kinetics can be described only by nucleation processes will help on clarifying this point on the geometrical impingement.

Acknowledgements

This work was supported by the Ministry of Science and Innovation (MICINN) and EU FEDER (project no. MAT2007-65227) and the PAI of the Regional Government of Andalucía (project no. P06-FQM-01823).

References

[1] Y. Yoshizawa, S. Oguma, K. Yamauchi, J. Appl. Phys. 64 (1988) 6044.
[2] K. Suzuki, A. Makino, N. Kataoka, A. Inoue, T. Masumoto, Mater. Trans. JIM 32 (1991) 93.
[3] M.A. Willard, D.E. Laughlin, M.E. McHenry, D. Thoma, K. Sickafus, J.O. Cross, V.G. Harris, J. Appl. Phys. 84 (1998) 6773.
[4] A. Hernando, M. Vázquez, T. Kulik, C. Prados, Phys. Rev. B 51 (1995) 3581.
[5] A. Inoue, Prog. Mater. Sci. 43 (1998) 365.
[6] D. Zander, U. Köster, Mater. Sci. Eng. A 375–377 (2004) 53.
[7] K. Hono, Prog. Mater. Sci. 47 (2002) 621.
[8] J.S. Blázquez, M. Millán, C.F. Conde, A. Conde, Phys. Stat. Sol. (a) 207 (2010) 1148.
[9] J.W. Christian, The Theory of Transformation in Metals and Alloys, Pergamon, Oxford, 1975.
[10] M.T. Clavaguera-Mora, N. Clavaguera, D. Crespo, T. Pradell, Prog. Mater. Sci. 47 (2002) 559.
[11] D.H. Ping, Y.Q. Wu, K. Hono, M.A. Willard, M.E. McHenry, D.E. Laughlin, Scr. Mater. 45 (2001) 781.
[12] Y. Zhang, J.S. Blázquez, A. Conde, P.J. Warren, A. Cerezo, Mater. Sci. Eng. A 353 (2003) 158.
[13] E. Jedryka, M. Wójcik, P. Svec, I. Skorvanek, Appl. Phys. Lett. 85 (2004) 2884.
[14] J.S. Blázquez, J.M. Borrego, C.F. Conde, A. Conde, J.M. Greneche, J. Phys.: Conden. Matter 15 (2003) 3957.
[15] M. Millán, J.S. Blázquez, C.F. Conde, A. Conde, S. Lozano-Pérez, J. Non-Cryst. Sol. 355 (2009) 109.
[16] J.M. Barandiarán, I. Tellería, J.S. Garitaonandía, H.A. Davies, J. Non-Cryst. Sol. 329 (2003) 57.
[17] P. Svec, P. Duhaj, Phys. Stat. Sol. (a) 105 (1988) 320.
[18] K. Kristiakova, P. Svec, Phys. Rev. B 64 (2001) 184202.
[19] J.S. Blázquez, M. Millán, C.F. Conde, A. Conde, Phil. Mag. 87 (2007) 4151.